Influence of the spin pumping induced inverse spin Hall effect on spin-torque ferromagnetic resonance measurements

Cite as: Appl. Phys. Lett. **118**, 132401 (2021); https://doi.org/10.1063/5.0038567
Submitted: 24 November 2020 . Accepted: 12 March 2021 . Published Online: 29 March 2021

Qi Liu, Y. Zhang, L. Sun, Bingfeng Miao, X. R. Wang, and H. F. Ding

Applied Physics Letters ARTICLE scitation.org/journal/apl

Influence of the spin pumping induced inverse spin Hall effect on spin-torque ferromagnetic resonance measurements

Cite as: Appl. Phys. Lett. **118**, 132401 (2021); doi: 10.1063/5.0038567
Submitted: 24 November 2020 · Accepted: 12 March 2021 ·
Published Online: 29 March 2021

Qi Liu,[1,2] Y. Zhang,[3,4] L. Sun,[1,2] Bingfeng Miao,[1,2,a)] X. R. Wang,[3,4,a)] and H. F. Ding[1,2,a)]

AFFILIATIONS

[1]National Laboratory of Solid State Microstructures and Department of Physics, Nanjing University, Nanjing 210093, People's Republic of China
[2]Collaborative Innovation Center of Advanced Microstructures, Nanjing 210093, People's Republic of China
[3]Physics Department, The Hongkong University of Science and Technology, Clear Water Bay, Kowloon, Hong Kong
[4]HKUST Shenzhen Research Institute, Shenzhen 518057, People's Republic of China

Note: This paper is part of the Special Topic on Spin-Orbit Torque (SOT): Materials, Physics and Devices.
[a)]**Authors to whom correspondence should be addressed:** bfmiao@nju.edu.cn; phxwan@ust.hk; and hfding@nju.edu.cn

ABSTRACT

Spin-torque ferromagnetic resonance (ST-FMR) has been widely used to determine the spin–orbit torque (SOT) efficiency in ferromagnet/heavy-metal bilayer systems. The flow of a radio frequency current through heavy-metal generates an oscillating SOT and Oersted field, resulting in the resonance of the adjacent ferromagnetic layer and subsequent dc voltage due to the rectification effect. The dynamics of the ferromagnet, however, also pumps a spin current back into the heavy-metal. Wherein, an additional contribution to the dc voltage arises from the inverse spin Hall effect (ISHE). The spin pumping-induced ISHE (SP-ISHE) and ST-FMR voltages typically have identical symmetry. In this work, we develop a method to quantitatively obtain the SP-ISHE voltage from the ST-FMR signal in the Py($Ni_{80}Fe_{20}$)/Pt bilayer. We find it has the opposite sign to the symmetric component of ST-FMR voltage. After this correction, both the damping-like and field-like-torque efficiency in the Py/Pt bilayer are further estimated through the Py-thickness-dependent measurements.

In current research of spintronic devices, the spin Hall effect (SHE)[1–3] is one of the most commonly used methods to generate pure spin current. It enables the conversion between charge and spin current without assistance of magnetic materials or magnetic field. At the ferromagnet/heavy-metal (FM/HM) interface, spin current exerts a spin–orbit torque (SOT) onto the ferromagnet.[4–7] This torque provides a promising mechanism to control magnetization dynamics of the ferromagnet.[5,7–10] It has also been recognized that SOT can manipulate the magnetization more efficiently than the magnetic field or the conventional spin transfer torque.[11–14] Therefore, the characterization and enhancement of SOT efficiency attract great attention in the spintronics community.

Spin-torque ferromagnetic resonance (ST-FMR) has been widely adopted to measure SOT efficiency in the FM/HM bilayer.[15–17] When a radio frequency (rf) current flows within the HM, it exerts an oscillating torque onto the FM layer due to the SHE. Although it is generally believed that the SHE mainly produces a damping-like torque, more and more investigations unveil that it also has a field-like torque component.[18–21] In addition, the Oersted field generated from the rf current also acts on the FM layer. Therefore, there are two driving forces for the magnetization precession, the SOT and the Oersted field. When the frequency of the rf current and the applied external magnetic field satisfies the ferromagnetic resonance (FMR) condition, the magnetization of the FM layer precesses. This results in a resistance oscillation due to the magnetoresistance of the FM layer. Consequently, a rectified dc voltage is generated due to the interplay of the oscillating current and resistance.[22–24] Importantly, the line shape of the voltage curve due to the damping-like torque is Lorentzian symmetric, while that from the field-like torque (both the SHE and Oersted field origin) is anti-symmetric. Thus, one can obtain the SOT efficiency from line shape analysis of the ST-FMR voltage curve.

In the ST-FMR experiment, the precession of FM moments also acts as the source of an angular momentum flow, which pumps a pure spin current into its neighboring HM.[25–28] Wherein, an additional

contribution to the dc voltage arises from the inverse spin Hall effect (ISHE),[28] which has a Lorentzian symmetric line shape. Both the SOT and spin pumping-induced ISHE (SP-ISHE) are proportional to the spin Hall angle of the HM. Thus, it was believed that the SP-ISHE was a second order effect of the rf current and significantly smaller than the ST-FMR signal.[15] However, the Oersted field induced by the rf current can also drive the precession of FM moment, resulting in non-negligible SP-ISHE contribution.[29] Recently, the artifact from the SP-ISHE in the ST-FMR technique has been realized. For instance, Kondou *et al.*[30] and Okada *et al.*[31] calculated the SP-ISHE contribution in the total ST-FMR signal, assuming these two have the same sign. They found non-negligible contribution of the ISHE when the anisotropic magnetoresistance (AMR) of the FM layer is small. Karimeddiny *et al.*[32] analyzed the angular dependence of both the longitudinal and transverse signals in the ST-FMR experiment and found that the sign of the SP-ISHE and the symmetric component of ST-FMR voltage is opposite.

In this work, we develop a method to quantitatively separate the SP-ISHE signal from the ST-FMR signal without tedious symmetry analysis. We identify that both the ST-FMR and SP-ISHE signals are proportional to the product of the in-plane and out-of-plane precession angles of the FM, i.e., $\alpha_1\beta_1$. After characterizing the precession angles in both setups via the microwave photoresistance measurements,[29,33–35] we directly obtain the SP-ISHE contribution in ST-FMR. Our method does not rely on many unknown parameters such as the spin diffusion length, spin Hall angle of the HM, and the effective spin-mixing conductance of FM-HM interface. Unexpectedly, we find that the SP-ISHE has the opposite sign to the symmetric component of ST-FMR for the Py($Ni_{80}Fe_{20}$)/Pt bilayer. Through the Py thickness-dependent measurements, we further estimate both the damping-like-torque and field-like-torque efficiency for the Py/Pt bilayer system.

We deposit a series of Py(t_{Py})/Pt(6 nm) bilayer thin films with $t_{Py} = 2 - 15$ nm onto the thermally oxidized silicon substrates with dc magnetron sputtering at room temperature. The samples are further patterned into two types of devices, 20 μm × 100 μm (for the ST-FMR measurement) and 20 μm × 2200 μm (for the SP-ISHE measurement) stripes by photolithography and liftoff. The two types of samples are prepared on substrates cut from the same wafer and placed side-by-side during the film deposition from the same sputtering target. Therefore, they are expected to have the same properties except for the length. In the ST-FMR measurement, we inject an rf current through the Py/Pt bilayer and measure the dc voltage at the same time by using a bias tee [Fig. 1(a)]. The angle between the external in-plane magnetic field and the applied rf current is φ. In the SP-ISHE measurement, the Py/Pt stripe is placed in-between the signal line and ground line of a coplanar waveguide [Fig. 1(b)]. In this geometry, the microwave magnetic field is mainly along the out-of-plane direction. The magnetic field is applied within the sample plane but perpendicular to the stripe direction. Under this configuration, the SP-ISHE signal is maximized and the unwanted parasite signal is minimized.[29] In order to achieve a high signal-to-noise ratio, we modulate the microwave with a frequency of 17.906 kHz and detect the voltage with a lock-in amplifier. All these measurements are performed at room temperature.

In the ST-FMR measurement, an rf charge current density $J_{Pt} = \mathrm{Re}(j_{Pt}e^{-i\omega t})$ that flows within the Pt layer produces an rf spin

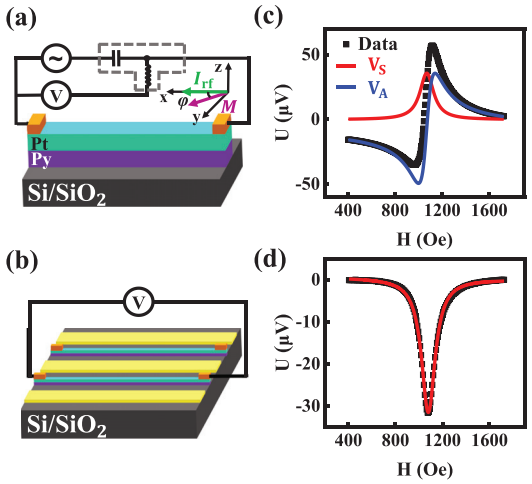

FIG. 1. Schematic illustration of the measurement setup of (a) the ST-FMR and (b) the SP-ISHE. (c) The ST-FMR signal of the Py(6 nm)/Pt(6 nm) sample at 9 GHz. The experimental data (black symbols) can be decomposed into symmetric (red line) and antisymmetric (blue line) Lorentzian components. (d) The SP-ISHE signal (black symbols) of the Py(6 nm)/Pt(6 nm) sample at 9 GHz. The red line is the fitting with the symmetric Lorentzian function.

current density $J_s = \mathrm{Re}(j_s e^{-i\omega t})$ because of the SHE of Pt. This will induce a spin–orbit torque $\boldsymbol{\tau}$ acting on the magnetic moment of Py, with $\boldsymbol{\tau} = -\gamma\xi_{DL}a\boldsymbol{m} \times (\boldsymbol{m} \times \boldsymbol{\sigma}) + \gamma\xi_{FL}a\boldsymbol{m}\times\boldsymbol{\sigma}$.[36,37] Here, ξ_{DL} and ξ_{FL} are the dimensionless damping-like-torque and field-like-torque efficiency, respectively. $\boldsymbol{m}$ describes the normalized magnetic moment of FM, $\boldsymbol{\sigma}$ is the spin direction, and $a = \frac{\hbar j_{Pt}}{2e\mu_0 M_S t_{Py}}$ with $\hbar$, e, μ_0, and M_S being the reduced Planck constant, the magnitude of the electron charge, the vacuum permeability, and the saturation magnetization of Py. In addition, the rf charge current also induces an rf Oersted field $\mathrm{Re}(\boldsymbol{h}_{rf}e^{-i\omega t})$ that acts on the magnetic moment of Py, determined by Ampère's law with $\boldsymbol{h}_{rf} = \frac{t_{Pt}}{2}\boldsymbol{j}_{Pt}\times\hat{z}$, where t_{Pt} is the thickness of the Pt layer. Therefore, the dynamics of the Py magnetic moment can be described by the generalized Landau-Lifshitz-Gilbert (LLG) equation:

$$\frac{d\boldsymbol{m}}{dt} = -\gamma\boldsymbol{m} \times (\boldsymbol{H}_{eff} + \boldsymbol{h}_{rf}) + \alpha\boldsymbol{m} \times \frac{\partial\boldsymbol{m}}{\partial t} + \boldsymbol{\tau}, \tag{1}$$

where γ is the gyromagnetic ratio, α is the Gilbert damping coefficient, and $\boldsymbol{H}_{eff}$ is the effective field. We further rewrite Eq. (1) as

$$\frac{d\boldsymbol{m}}{dt} = -\gamma\boldsymbol{m} \times (\boldsymbol{h}_{rf} - \xi_{FL}a\boldsymbol{\sigma}) - \gamma\xi_{DL}a\boldsymbol{m} \times (\boldsymbol{m} \times \boldsymbol{\sigma}) - \gamma\boldsymbol{m} \times \boldsymbol{H}_{eff} + \alpha\boldsymbol{m} \times \frac{\partial\boldsymbol{m}}{\partial t}. \tag{2}$$

On the right side, the first and second terms correspond to the field-like torque (including both SOT and the Oersted field) and damping-like torque, respectively. When Py is driven into a steady precession state, its resistance oscillates with the same frequency of the rf current. The interplay between the rf current and the oscillating resistance results in a dc rectification voltage. For the Py/Pt bilayer, both AMR and spin Hall magnetoresistance (SMR)[38] contribute to the rectified voltage. However, when the magnetization of Py rotates within the *xy*-plane, SMR has exactly the same angular dependence as AMR. The

unidirectional spin Hall magnetoresistance (USMR) is around two orders' of magnitude smaller than AMR.[39] Thus, in the absence of the spin pumping-induced ISHE, the measured signal can be written as

$$V_{\mathrm{mix}} = -\frac{I_{\mathrm{rf}} R_M}{2\alpha(2H_0 + 4\pi M_{\mathrm{eff}})}\left[SF_{\mathrm{S}}(H_{\mathrm{ext}}) + AF_{\mathrm{A}}(H_{\mathrm{ext}})\right]\sin 2\varphi\cos\varphi. \tag{3}$$

Here, $F_{\mathrm{S}}(H_{\mathrm{ext}}) = \frac{\Delta H^2}{(H-H_0)^2+\Delta H^2}$ and $F_{\mathrm{A}}(H_{\mathrm{ext}}) = \frac{\Delta H(H-H_0)}{(H-H_0)^2+\Delta H^2}$ are the symmetric and antisymmetric Lorentzian functions centered at the resonant field H_0 with linewidth ΔH. I_{rf} is the rf current flowing within the sample, R_M is the magnetoresistance of the sample (including AMR and SMR), and M_{eff} is the effective magnetization of Py. In addition, $S = a\xi_{\mathrm{DL}}$ and $A = (a\xi_{\mathrm{FL}} + \frac{1}{2}j_{\mathrm{Pt}}t_{\mathrm{Pt}})\sqrt{(H_0+4\pi M_{\mathrm{eff}})/H_0}$. Therefore, the ST-FMR signal has a symmetric Lorentzian component (V_{S}) proportional to the damping-like torque induced by J_{s} and an antisymmetric Lorentzian component (V_A) proportional to the sum of $\boldsymbol{h}_{\mathrm{rf}}$ and the field-like torque induced by J_{s}. Figure 1(c) presents the field-dependent ST-FMR signal of Py(6 nm)/Pt(6 nm), where a 9-GHz rf current with 23 dBm amplitude is injected into the bilayer. The signal can be well fitted by a combination of symmetric (red line) and antisymmetric (blue line) Lorentzian components. We note that when the microwave is injected into the Py/Pt stripe, Joule heating would raise the sample temperature and induce thermoelectric signals. Because additional heat dissipation at the FMR condition is negligible, these thermoelectric voltages only serve as a background and do not contaminate ST-FMR as long as the resonance field is sufficiently larger than the saturation field of Py.[40]

To simplify the discussion, we define an effective parameter $\xi_{\mathrm{FMR}} = \frac{S}{A}\frac{e\mu_0 M_{\mathrm{S}} t_{\mathrm{Py}} t_{\mathrm{Pt}}}{\hbar}\sqrt{(H_0+4\pi M_{\mathrm{eff}})/H_0}$.[15] For Py(6 nm)/Pt(6 nm), we obtain $\xi_{\mathrm{FMR}} = 0.050$. From Eq. (3), we have

$$\frac{1}{\xi_{\mathrm{FMR}}} = \frac{1}{\xi_{\mathrm{DL}}}\left(1 + \frac{\hbar}{e\,\mu_0 M_{\mathrm{S}} t_{\mathrm{Py}} t_{\mathrm{Pt}}}\frac{\xi_{\mathrm{FL}}}{}\right). \tag{4}$$

Therefore, both ξ_{DL} and ξ_{FL} can be derived from Py thickness-dependent measurements. The above discussion is valid only when the spin pumping-induced ISHE is negligible. In the following, we will discuss the influence of the SP-ISHE on the ST-FMR measurement.

In the FMR condition, Py also pumps a spin current back into Pt, where it is converted into charge current via the ISHE. As presented in Fig. 1(d), the SP-ISHE signal has a symmetric Lorentzian line shape, the same as the damping-like-torque contribution in the ST-FMR. Thus, it is pivotal to isolate the SP-ISHE from ST-FMR in order to obtain the correct ξ_{DL} and ξ_{FL} values. After taking into account the spin backflow, the normalized SP-ISHE dc voltage can be described as[35,41,42]

$$\frac{V_{\mathrm{ISHE}}^{\mathrm{SP}}}{\alpha_1\beta_1 R_{\mathrm{FN}} few\sin\varphi} \propto \eta\theta_{\mathrm{SH}}\lambda_{\mathrm{sd}}\tanh\frac{t_{\mathrm{Pt}}}{2\lambda_{\mathrm{sd}}}, \tag{5}$$

where η describes the FM/HM interface properties, f is the microwave frequency, R_{FN} is the resistance of bilayer, w is the strip width, θ_{SH} and λ_{sd} are the spin Hall angle and spin diffusion length of Pt, respectively. In the ST-FMR geometry, both the spin polarization due to SHE and the Oersted field are along the y direction. Thus, both the in- and out-of-plane precession angles α_1 and β_1 of Py have the angular dependence of $\cos\varphi$. In addition, the ISHE depends on the Py magnetization with $\sin\varphi$. In together, the SP-ISHE is proportional to $\sin 2\varphi\cos\varphi$, indistinguishable to both V_{S} and V_A of the ST-FMR signal [Eq. (3)].

Figure 2(a) presents the angular dependence of V_{S} and V_A in the ST-FMR measurements. Overall, both curves can be well fitted with $\sin 2\varphi\cos\varphi$ function. Interestingly, we find V_{S} of the detected ST-FMR signal is negative when φ is around $-90°$, as also presented in Fig. 2(b). This is unexpected since $-\sin 2\varphi\cos\varphi \geq 0$ when $\varphi \in [-180°, 0°]$. Thus, the abnormal behavior of V_{S} cannot be explained by the ST-FMR and SP-ISHE induced by in-plane microwave magnetic field h_{y} only. In fact, when the charge current flows along the x-direction, there is inevitably z-component magnetic field near the stripe edge. Since the SP-ISHE is proportional to the square of the rf field, the effect of the z-component would not cancel each other even though they have different signs at the opposite edges. The non-zero symmetric component near $\varphi = -90°$ can therefore be understood by the SP-ISHE due to the out-of-plane microwave magnetic field h_z, which is proportional to $\sin\varphi$. The small antisymmetric component is from ST-FMR because of limited angle resolution [Fig. 2(b)]. Indeed, we also find that V_{S} of ST-FMR is positive when φ is around 90° where $-\sin 2\varphi\cos\varphi \leq 0$. As a control sample, the SP-ISHE signal of the Pt/Py bilayer excited by h_z indeed has an opposite sign with V_{S} of ST-FMR [Figs. 1(c) and 1(d)]. Although the SP-ISHE due to h_z is about two orders of magnitude smaller than the ST-FMR signal, it is important to note that h_z is also much smaller than the dominant h_{y}. Therefore, the SP-ISHE excited by in-plane h_{y} in the ST-FMR measurement could be non-negligible. The SP-ISHE voltage is opposite with V_{S} of ST-FMR, since the sign of the SP-ISHE is irrelevant with the direction of the rf magnetic field. Thus, the SOT efficiency measured in the Py/Pt bilayer is underestimated in the ST-FMR measurements.

Since the ST-FMR and SP-ISHE excited by h_{y} all share the same angular dependence, it is not straightforward to distinguish them from the symmetry analysis. From Eq. (5), we find that for the samples of the same materials with the same structure and thickness, the value of $\frac{V_{\mathrm{ISHE}}^{\mathrm{SP}}}{\alpha_1\beta_1 R_{\mathrm{FN}} few\sin\varphi}$ is a constant. Thus, when we fabricate two identical samples with the same width but different lengths and perform the ST-FMR and spin pumping measurements with the same rf frequency, the SP-ISHE voltages in these two configurations satisfy $\frac{V_{\mathrm{ISHE}}^{\mathrm{ST-FMR}}}{\alpha_1^{\mathrm{ST-FMR}}\beta_1^{\mathrm{ST-FMR}}R_{\mathrm{FN}}^{\mathrm{ST-FMR}}\sin\varphi^{\mathrm{ST-FMR}}} = \frac{V_{\mathrm{ISHE}}^{\mathrm{SP-ISHE}}}{\alpha_1^{\mathrm{SP-ISHE}}\beta_1^{\mathrm{SP-ISHE}}R_{\mathrm{FN}}^{\mathrm{SP-ISHE}}\sin\varphi^{\mathrm{SP-ISHE}}}$. By determining the precession angles α_1 and β_1, we can directly obtain the SP-ISHE contribution in the ST-FMR measurements. The precession angles can be measured via the microwave photoresistance

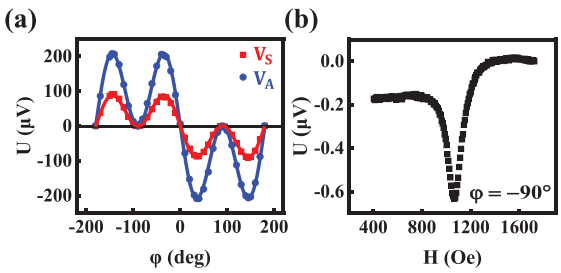

FIG. 2. (a) The angular-dependent V_{S} (red symbols) and V_A (blue symbols) of the measured signal of Py(6 nm)/Pt(6 nm) in ST-FMR measurements. Lines are fittings using the $\sin 2\varphi\cos\varphi$ function. (b) The field-dependent signal at $\varphi = -90°$.

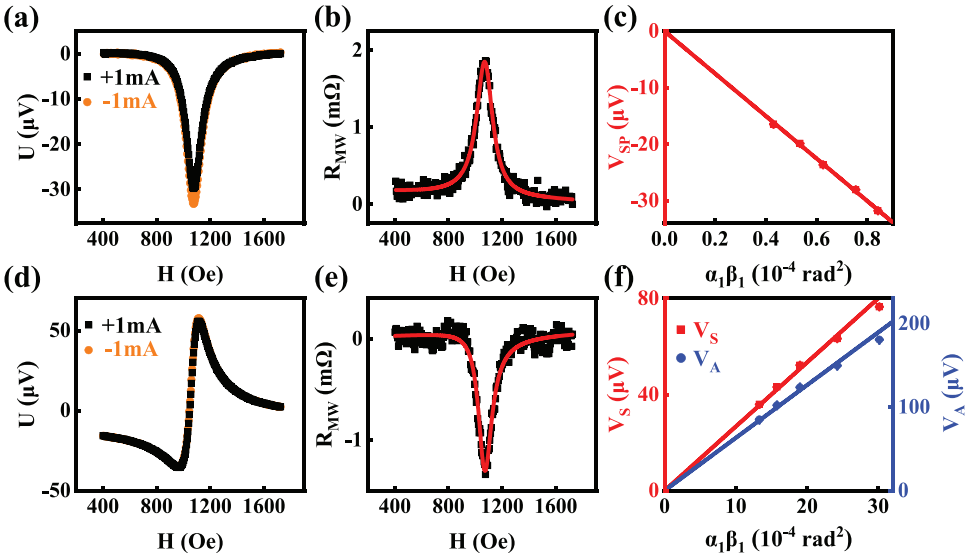

FIG. 3. (a), (b), and (c) are the measurements with the SP-ISHE configuration at $\varphi = -90°$, f=9 GHz and (d), (e), and (f) are the measurements with the ST-FMR configuration at $\varphi = -10°$, f = 9 GHz. (a) and (d) are the magnetic field-dependent voltages of the Py(6 nm)/Pt(6 nm) sample with dc current $+I_0$ (+1 mA, black curve) and $-I_0$ (−1 mA, orange curve). (b) and (e) are the magnetic field-dependent microwave photoresistance. (c) and (f) are the relationship between the measured voltage signals and the product of the in-plane and out-of-plane precession angles.

measurement.[29,33] Figure 3(a) presents the field-dependent voltage curves for the Py(6 nm)/Pt(6 nm) sample in the spin pumping measurement, with the dc current $+I_0$ (+1 mA, black) and $-I_0$ (−1 mA, orange), respectively. The external magnetic field is applied along $\varphi = -90°$, and the microwave is 9 GHz with 32 dBm. In the FMR condition, the magnetization precession alters the angle of the magnetization with respect to the dc current, resulting in a change of the time-averaged resistance due to the MR. This is the so-called microwave photoresistance R_{MW}.[43] Figure 3(b) presents R_{MW} obtained by $R_{MW} = \frac{U(+I_0)-U(-I_0)}{2I_0}$, and it can be described with

$$R_{MW}(H_{ext}) = -\frac{R_M}{2}(\alpha_1^2 \cos 2\varphi + \beta_1^2 \cos^2\varphi) \times F_S(H_{ext}). \quad (6)$$

Here, $\alpha_1/\beta_1 = \sqrt{1 + 4\pi M_{eff}/H_0}$. Fitting the data with Eq. (6), we obtain $\alpha_1 = 0.016\,rad$, $\beta_1 = 0.005\,rad$, respectively. For a given sample with a fixed microwave frequency, the V_{SP} indeed scales linearly with product of $\alpha_1\beta_1$ by varying the microwave power [Fig. 3(c)]. Similarly, we also perform the microwave photoresistance measurement in the ST-FMR geometry at $\varphi = -10°$, where both ST-FMR and R_{MW} are relatively large. Figure 3(d) presents the ST-FMR curves for Py(6 nm)/Pt(6 nm) with ±1 mA dc current. The injected rf current is 9 GHz with 23 dBm. In this geometry, the precession angles are obtained as α_1=0.062 *rad*, β_1=0.022 *rad* [Fig. 3(e)]. The SP-ISHE voltage in the ST-FMR measurement can thus be calculated as ∼−4.2 μV, where the symmetric component of ST-FMR signal V_S is 35.9 μV [Fig. 1(c)]. The contribution of SP-ISHE voltage in the ST-FMR signal is ∼12%. After removing this SP-ISHE signal, we correct the value of ξ_{FMR} from 0.050 to 0.056. As expected, both V_S and V_A of the ST-FMR signal also increase linearly with the product of the in-plane and out-of-plane precession angles $\alpha_1\beta_1$ [Fig. 3(f)].

Finally, we obtain the damping-like-torque efficiency ξ_{DL} and the field-like-torque efficiency ξ_{FL} in the Py/Pt bilayer system. According to Eq. (4), $\frac{1}{\xi_{FMR}}$ is linearly proportional to $\frac{1}{\mu_0 M_S t_{Py}}$, where ξ_{DL} and ξ_{FL} can be determined from the intercept and slope. We thus perform the ST-FMR measurements on a series of Py(t_{Py})/Pt(6 nm) with different Py thicknesses. From the microwave frequency-dependent resonance field, thickness-dependent magnetization $4\pi M_{eff}$ of Py can be obtained using the Kittel equation [Fig. 4(a)]. Figure 4(b) presents the hysteresis loops of Py(t_{Py})/Pt(6 nm) bilayers with the superconducting quantum interference device-vibrating sample magnetometer. The $4\pi M_S$ as a function of Py is also plotted in Fig. 4(a). $4\pi M_{eff}$ and $4\pi M_S$ have similar values except for 2-nm Py, indicating a weak interface anisotropy.

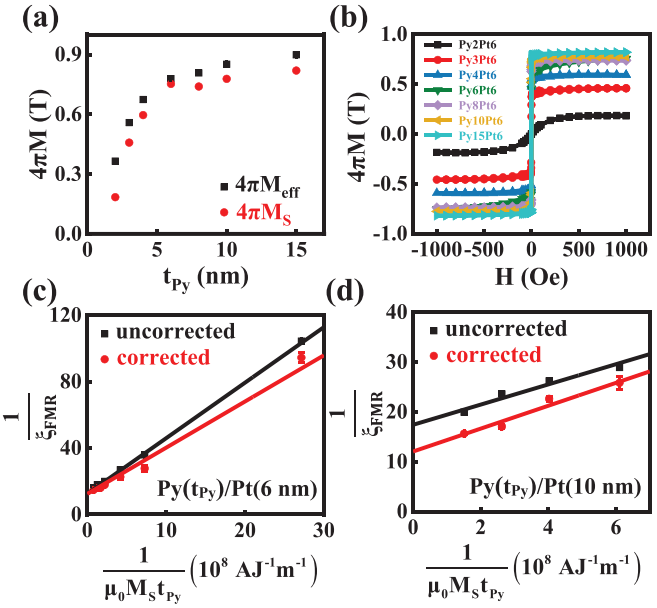

FIG. 4. (a) t_{Py}-dependent effective saturation magnetization $4\pi M_{eff}$ (black) and saturation magnetization $4\pi M_S$ (red) of Py. (b) Hysteresis loops of a series of Py(t_{Py})/Pt(6 nm) bilayers. Corrected (red) and uncorrected (black) $\frac{1}{\xi_{FMR}}$ vs $\frac{1}{\mu_0 M_S t_{Py}}$ for (c) Py(t_{Py})/Pt(6 nm) system, and (d) Py(t_{Py})/Pt(10 nm) system. The lines are fittings with Eq. (4).

TABLE I. Comparison of ξ_{DL} and ξ_{FL} obtained among different groups.

System	Py/Pt[44]	CoFeB/Pt[32]	CoFeB/Pt[45]	Ta/Fe/Pt[46]	Py/Pt (this work)
ξ_{DL}	0.087 ± 0.007	0.090 ± 0.006	0.09	0.12 ± 0.02	0.083 ± 0.005
ξ_{FL}	0.024 ± 0.003	-0.020 ± 0.002	N. A.	N. A.	0.023 ± 0.003

With the help of microwave photoresistance measurements, we further correct the SOT efficiency taking into account the SP-ISHE contribution for every sample. Figure 4(c) presents the corrected and uncorrected $\frac{1}{\xi_{FMR}}$ as a function of $\frac{1}{\mu_0 M_S t_{Py}}$. The linear fitting yields damping-like-torque efficiency $\xi_{DL} = 0.081 \pm 0.002$ and field-like-torque efficiency $\xi_{FL} = 0.020 \pm 0.002$ for the Py(t_{Py})/Pt(6 nm) system. To check the consistency, we also performed similar studies to 10-nm Pt [Fig. 4(d)]. The contribution of the SP-ISHE to the measured symmetrical signal increases sharply as compared to 6-nm Pt. The obtained SOT efficiencies are $\xi_{DL} = 0.084 \pm 0.007$ and $\xi_{FL} = 0.025 \pm 0.004$, consistent with those obtained with 6-nm Pt within the experimental error margin. By averaging these values obtained with different Pt thicknesses, we have $\xi_{DL} = 0.083 \pm 0.005$ and $\xi_{FL} = 0.023 \pm 0.003$. As presented in Table I, both ξ_{DL} and ξ_{FL} are in excellent agreement with those obtain by Nan *et al.* for the Py/Pt system.[44] ξ_{DL} is also consistent with the values reported by Karimeddiny *et al.*[32] and Skowronski *et al.*[45] for the CoFeB/Pt bilayer system, albeit smaller than the value reported by Liu *et al.*[46] for the Ta(4 nm)/Fe(4 nm)/Pt(5 nm) trilayer system. The difference may due to the fact that no FL torque correction was considered in that work, and the Pt/Fe sample was deposited on Ta buffer layer, which also had strong spin–orbit coupling thus might influence the result. We note that the obtained ξ_{FL} has opposite sign with CoFeB/Pt bilayer system,[32] suggesting it is interface-dependent and provides additional opportunity to tune the efficiency with interface engineering in the SOT-based devices.

In conclusion, we develop a method to separate the SP-ISHE signal from the ST-FMR voltage. In combination with the precession angle measurements, we can quantitatively isolate the SP-ISHE signal in the ST-FMR technique. The contribution of SP-ISHE voltage to the symmetric component of the ST-FMR signal is non-negligible and with opposite signs. After correction, we obtain the damping-like-torque efficiency ξ_{DL} and field-like-torque efficiency ξ_{FL} of the Py/Pt bilayer to be 0.083 ± 0.005 and 0.023 ± 0.003, respectively.

This work was supported by the National Key R&D Program of China (Grant Nos. 2018YFA0306004 and 2017YFA0303202); the National Natural Science Foundation of China (Grant Nos. 51971110, 11974165, 11734006, and 11727808); and the Natural Science Foundation of Jiangsu Province (Grant No. BK20190057). X.R.W. was supported by the National Natural Science Foundation of China (Grant No. 11774296) and Hong Kong RGC (Grant Nos. 16301518 and 16301619).

DATA AVAILABILITY

The data that support the findings of this study are available from the corresponding author upon reasonable request.

REFERENCES

[1]A. Hoffmann, IEEE Trans. Magn. **49**, 5172 (2013).
[2]J. Sinova, S. O. Valenzuela, J. Wunderlich, C. H. Back, and T. Jungwirth, Rev. Mod. Phys. **87**, 1213 (2015).
[3]Y. Niimi and Y. Otani, Rep. Prog. Phys. **78**, 124501 (2015).
[4]I. M. Miron, K. Garello, G. Gaudin, P. J. Zermatten, M. V. Costache, S. Auffret, S. Bandiera, B. Rodmacq, A. Schuhl, and P. Gambardella, Nature **476**, 189 (2011).
[5]R. Ramaswamy, J. M. Lee, K. Cai, and H. Yang, Appl. Phys. Rev. **5**, 031107 (2018).
[6]A. Manchon, J. Železný, I. M. Miron, T. Jungwirth, J. Sinova, A. Thiaville, K. Garello, and P. Gambardella, Rev. Mod. Phys. **91**, 035004 (2019).
[7]C. Song, R. Zhang, L. Liao, Y. Zhou, X. Zhou, R. Chen, Y. You, X. Chen, and F. Pan, Prog. Mater. Sci. **118**, 100761 (2021).
[8]P. Gambardella and I. M. Miron, Philos. Trans. R. Soc., A **369**, 3175 (2011).
[9]Y. Li, K. W. Edmonds, X. Liu, H. Zheng, and K. Wang, Adv. Quantum Technol. **2**, 1800052 (2019).
[10]J. Ryu, S. Lee, K. J. Lee, and B. G. Park, Adv. Mater. **32**, 1907148 (2020).
[11]J. Slonczewski, J. Magn. Magn. Mater. **159**, L1 (1996).
[12]D. C. Ralph and M. D. Stiles, J. Magn. Magn. Mater. **320**, 1190 (2008).
[13]J. A. Katine, F. J. Albert, R. A. Buhrman, E. B. Myers, and D. C. Ralph, Phys. Rev. Lett. **84**, 3149 (2000).
[14]S. I. Kiselev, J. C. Sankey, I. N. Krivorotov, N. C. Emley, R. J. Schoelkopf, R. A. Buhrman, and D. C. Ralph, Nature **425**, 380 (2003).
[15]L. Liu, T. Moriyama, D. C. Ralph, and R. A. Buhrman, Phys. Rev. Lett. **106**, 036601 (2011).
[16]W. Zhang, W. Han, X. Jiang, S.-H. Yang, and S. S. P. Parkin, Nat. Phys. **11**, 496 (2015).
[17]A. R. Mellnik, J. S. Lee, A. Richardella, J. L. Grab, P. J. Mintun, M. H. Fischer, A. Vaezi, A. Manchon, E. A. Kim, N. Samarth, and D. C. Ralph, Nature **511**, 449 (2014).
[18]S. Zhang, P. M. Levy, and A. Fert, Phys. Rev. Lett. **88**, 236601 (2002).
[19]J. Kim, J. Sinha, M. Hayashi, M. Yamanouchi, S. Fukami, T. Suzuki, S. Mitani, and H. Ohno, Nat. Mater. **12**, 240 (2013).
[20]K. W. Kim, S. M. Seo, J. Ryu, K. J. Lee, and H. W. Lee, Phys. Rev. B **85**, 180404 (2012).
[21]K. Garello, I. M. Miron, C. O. Avci, F. Freimuth, Y. Mokrousov, S. Blügel, S. Auffret, O. Boulle, G. Gaudin, and P. Gambardella, Nat. Nanotechnol. **8**, 587 (2013).
[22]A. A. Tulapurkar, Y. Suzuki, A. Fukushima, H. Kubota, H. Maehara, K. Tsunekawa, D. D. Djayaprawira, N. Watanabe, and S. Yuasa, Nature **438**, 339 (2005).
[23]J. C. Sankey, P. M. Braganca, A. G. F. Garcia, I. N. Krivorotov, R. A. Buhrman, and D. C. Ralph, Phys. Rev. Lett. **96**, 227601 (2006).
[24]H. Kubota, A. Fukushima, K. Yakushiji, T. Nagahama, S. Yuasa, K. Ando, H. Maehara, Y. Nagamine, K. Tsunekawa, D. D. Djayaprawira, N. Watanabe, and Y. Suzuki, Nat. Phys. **4**, 37 (2008).
[25]Y. Tserkovnyak, A. Brataas, and G. E. W. Bauer, Phys. Rev. B **66**, 224403 (2002).
[26]E. Saitoh, M. Ueda, H. Miyajima, and G. Tatara, Appl. Phys. Lett. **88**, 182509 (2006).
[27]M. V. Costache, M. Sladkov, S. M. Watts, C. H. van der Wal, and B. J. van Wees, Phys. Rev. Lett. **97**, 216603 (2006).
[28]O. Mosendz, V. Vlaminck, J. E. Pearson, F. Y. Fradin, G. E. W. Bauer, S. D. Bader, and A. Hoffmann, Phys. Rev. B **82**, 214403 (2010).
[29]Z. Feng, J. Hu, L. Sun, B. You, D. Wu, J. Du, W. Zhang, A. Hu, Y. Yang, D. M. Tang, B. S. Zhang, and H. F. Ding, Phys. Rev. B **85**, 214423 (2012).
[30]K. Kondou, H. Sukegawa, S. Kasai, S. Mitani, Y. Niimi, and Y. Otani, Appl. Phys. Express **9**, 023002 (2016).

[31]A. Okada, Y. Takeuchi, K. Furuya, C. Zhang, H. Sato, S. Fukami, and H. Ohno, Phys. Rev. Appl. **12**, 014040 (2019).
[32]S. Karimeddiny, J. A. Mittelstaedt, R. A. Buhrman, and D. C. Ralph, Phys. Rev. Appl. **14**, 024024 (2020).
[33]N. Mecking, Y. S. Gui, and C. M. Hu, Phys. Rev. B **76**, 224430 (2007).
[34]A. Yamaguchi, K. Motoi, A. Hirohata, H. Miyajima, Y. Miyashita, and Y. Sanada, Phys. Rev. B **78**, 104401 (2008).
[35]X. Tao, Q. Liu, B. F. Miao, R. Yu, Z. Feng, L. Sun, B. You, J. Du, K. Chen, S. Zhang, L. Zhang, Z. Yuan, D. Wu, and H. F. Ding, Sci. Adv. **4**, eaat1670 (2018).
[36]C. F. Pai, Y. Ou, L. H. Vilela-Leão, D. C. Ralph, and R. A. Buhrman, Phys. Rev. B **92**, 064426 (2015).
[37]Y. Zhang, Q. Liu, B. F. Miao, H. F. Ding, and X. R. Wang, Phys. Rev. B **99**, 064424 (2019).
[38]H. Nakayama, M. Althammer, Y. T. Chen, K. Uchida, Y. Kajiwara, D. Kikuchi, T. Ohtani, S. Geprägs, M. Opel, S. Takahashi, R. Gross, G. E. W. Bauer, S. T. B. Goennenwein, and E. Saitoh, Phys. Rev. Lett. **110**, 206601 (2013).
[39]C. O. Avci, K. Garello, A. Ghosh, M. Gabureac, S. F. Alvarado, and P. Gambardella, Nat. Phys. **11**, 570 (2015).
[40]J. Cheng, K. He, M. Yang, Q. Liu, R. Yu, L. Sun, J. Ding, B. Miao, M. Wu, and H. F. Ding, Phys. Rev. B **103**, 014415 (2021).
[41]K. Chen and S. Zhang, IEEE Magn. Lett. **6**, 3000304 (2015).
[42]K. Chen and S. Zhang, Phys. Rev. Lett. **114**, 126602 (2015).
[43]Y. S. Gui, N. Mecking, A. Wirthmann, L. H. Bai, and C. M. Hu, Appl. Phys. Lett. **91**, 082503 (2007).
[44]T. Nan, S. Emori, C. T. Boone, X. Wang, T. M. Oxholm, J. G. Jones, B. M. Howe, G. J. Brown, and N. X. Sun, Phys. Rev. B **91**, 214416 (2015).
[45]W. Skowroński, Ł. Karwacki, S. Ziętek, J. Kanak, S. Łazarski, K. Grochot, T. Stobiecki, P. Kuświk, F. Stobiecki, and J. Barnaś, Phys. Rev. Appl. **11**, 024039 (2019).
[46]E. Liu, T. Fache, D. Cespedes-Berrocal, Z. Zhang, S. Petit-Watelot, S. Mangin, F. Xu, and J. C. Rojas-Sánchez, Phys. Rev. Appl. **12**, 044074 (2019).